Technical Report 1635
February 1994

Active LFM Mixer Adaptive (ALMA) Beamforming

J. C. Lockwood

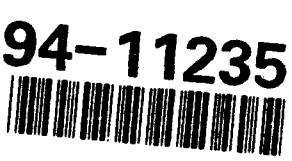

NRaD

Technical Report 1635
February 1994

Active LFM Mixer Adaptive (ALMA) Beamforming

J. C. Lockwood

NAVAL COMMAND, CONTROL AND OCEAN SURVEILLANCE CENTER
RDT&E DIVISION
San Diego, California 92152–5001

K. E. EVANS, CAPT, USN
Commanding Officer

R. T. SHEARER
Executive Director

ADMINISTRATIVE INFORMATION

This work was conducted during FY 1993 under project RJ14B28 of the Wide Area Undersea Surveillance Block Program. This Block Program is managed by the Naval Command, Control and Ocean Surveillance Center, RDT&E Division, under the guidance and direction of the Office of Naval Research. This work was funded under program element 0602314N and was performed by members of the Processing Systems Branch, Code 734, Naval Command, Control and Ocean Surveillance Center, RDT&E Division, San Diego, CA 92152–5001.

This technology is covered by U. S. Patent #5,251,186 of 5 October 1993 assigned to the U. S. Government. Parties interested in licensing this technology may direct inquiries to:

Harvey Fendelman
Legal Counsel for Patents
Code 0012
NCCOSC
San Diego, CA 92152–5765
(619) 553–3001

Released by
J. C. Lockwood, Head
Processing Systems Branch

Under authority of
L. E. Griffith, Head
Signal and Information
Processing Division

MA

EXECUTIVE SUMMARY

OBJECTIVE

The Active LFM Mixer Adaptive (ALMA) beamformer concept, a novel technique that enables optimum beamforming of broadband active sonar signals within each independent range-resolution annulus, is described.

RESULTS

Results of simulations have demonstrated that theALMA algorithms can adapt to each range-resolution annulus and suppress sidelobe interference while preserving signals in the intended look direction. Methods of implementing spatial-smoothing for both element- and beam-based adaptive algorithms have been covered, as well as methods of applying ALMA to long arrays.

CONCLUSIONS

ALMA beamforming reduces the signal from each range-resolution cell at each array element to a single phase and amplitude (accomplished by the mixer) and applies minimum-energy adaptive methods to these quantities to adapt (without time- or range-averaging) to the scatterer distribution in each range-resolution annulus. This approach is, to the author's knowledge, a unique contribution to the field of adaptive beamforming for active signals. The effectiveness of the algorithm in improving the detectability of echoes through the suppression of sidelobe interference has been demonstrated by simulation.Based on results seen to date, ALMA beamforming offers the promise of increasing the effective array gain of modest-sized active receiving arrays to produce an effect equivalent to making the array several times longer.

CONTENTS

FIGURES

INTRODUCTION

The Active LFM Mixer Adaptive (ALMA) beamformer concept is a novel technique that enables optimum beamforming of broadband active sonar signals within each independent range-resolution annulus. Use of the linear frequency modulation (LFM) waveform allows the use of a mixer preprocessor to compress the pulse, mapping each range-resolution cell into a discrete cw signal. This mapping of range into frequency allows the signal in each resolution cell to be completely described by the amplitude and phase of the continuous wave (cw) signal in the corresponding frequency cell, and enables the use of beamforming techniques that are formally the same as narrowband, frequency-domain beamforming for this essentially time-domain process.

A minimum-energy adaptive beamforming (ABF) algorithm is applied to suppress sidelobe responses to strong, discrete scatterers that would otherwise tend to mask weaker scattering events at different angular positions within the same range annulus. Adaptation to a single range annulus means that signal parameters cannot generally be averaged over time. That such time-averaging is not required in the ALMA process represents a major difference from other active adaptive beamforming approaches that have typically relied on time-averaging to assemble enough independent signal information into the covariance estimate to enable the signal space to be adequately defined.

Figures 1 and 2 illustrate the advantage of the ALMA beamformer relative to conventional beamforming in imaging the spatial distribution of scatterers. The figures are three-dimensional plots of beamformer response versus azimuth and range, and are the results of simulating the conventional and ALMA beamforming processes applied to a field of scatterers specifically designed to produce a recognizable pattern at the beamformer output. In each figure, the ambiguous left half of the line-array azimuthal response has been replaced by the true scattering field. Thus, an ideal beamformer would produce a right half that was the mirror image of the true field on the left. The pattern formed by the scatterers resembles a marching band on the sea floor spelling out the mirror image of the word "ALMA." It is important to note that the scatterers forming one stroke of each character were given a target strength 13 dB higher than the remaining scatterers. Hence, the sidelobe responses to the strong scatterers will tend to obscure the pattern.

Figure 1 shows the result of applying conventional beamforming to the mixer output. This conventional beamformer is applied at the mixer output, and is therefore, a true broadband beamformer. As expected, the sidelobe responses to the strong scatterers effectively obscure the pattern.

Figure 2 depicts the ALMA beamformer response alongside the true distribution. Apparently, many of the weaker events that could not be seen in the conventional response are being imaged, and the word "ALMA" can be recognized. It is also apparent that the image is not perfect. The angular regions near endfire to the array show a reduced angular resolution, as well as some evidence of signal suppression. Signal suppression is an inherent problem in active ABF due to the correlated nature of the echoes from multiple scatterers. This problem is minimized by a spatial averaging technique previously developed for dealing with the effects of correlated multipath in passive ABF.

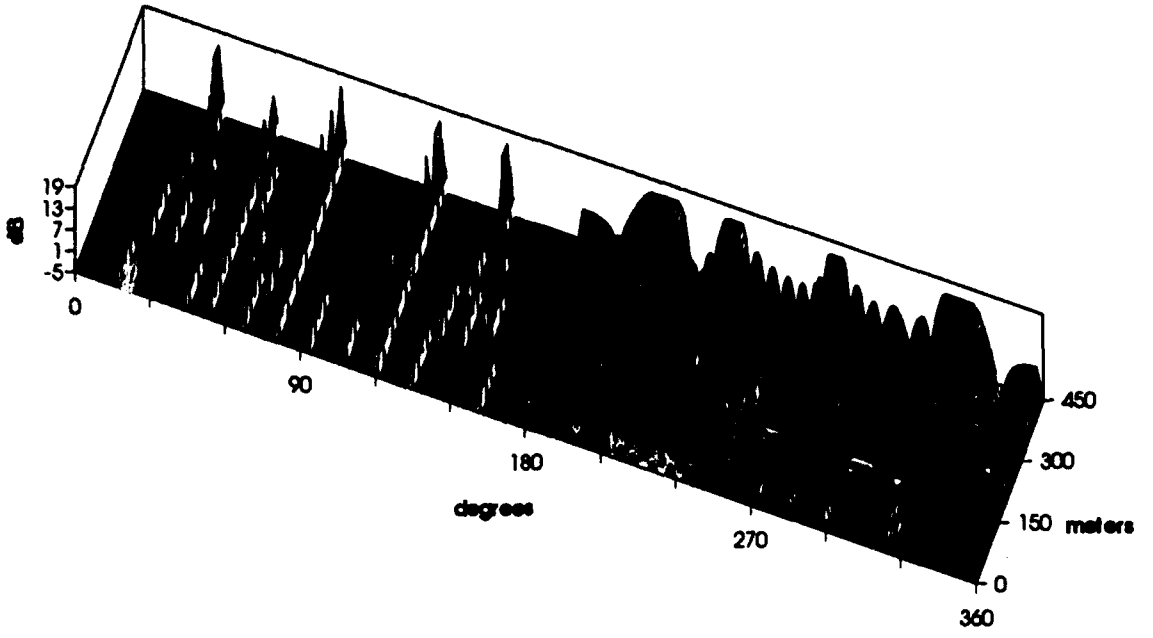

Figure 1. Conventional mixer beamformer response (right) to "ALMA" scattering field (left).

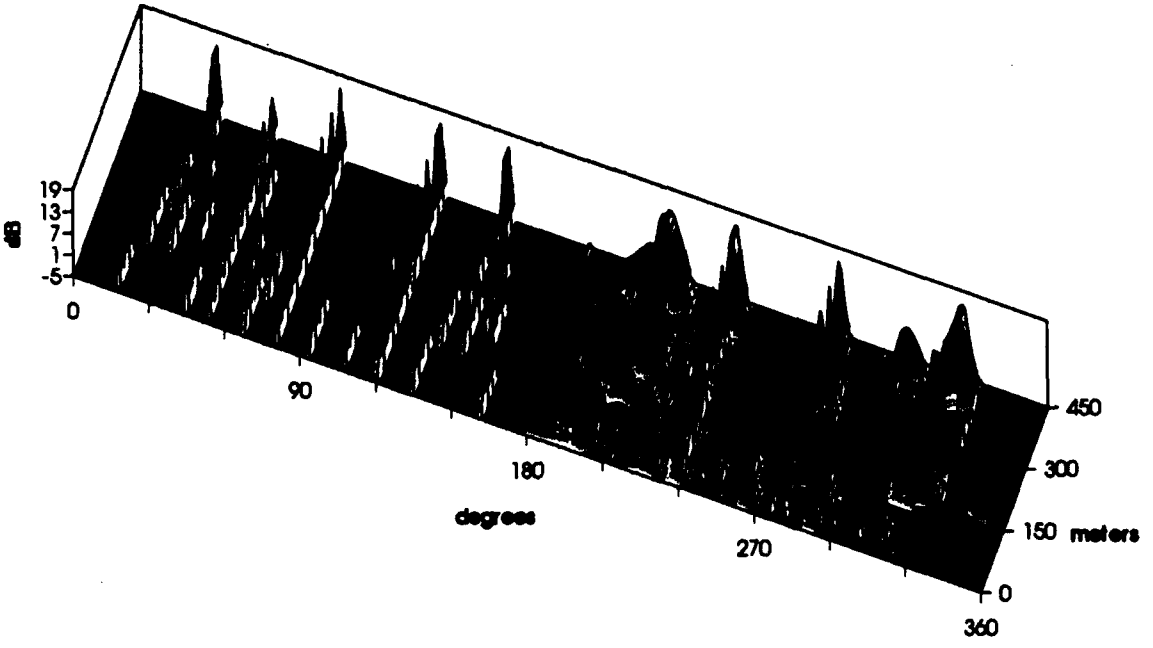

Figure 2. ALMA beamformer response (right) to "ALMA" scattering field (left).

By adapting to the scattering field within each range-resolution annulus, ALMA makes it possible to detect weak events that would otherwise be masked by sidelobe responses to strong scatterers at the same range.

The present report describes the ALMA algorithm and its variants. Results of simulations are presented that demonstrate the behavior of the conventional and adaptive mixer beamformer, and demonstrate the effectiveness of spatial smoothing in counteracting signal suppression. The report begins with a description of the mixer preprocessing and conventional beamforming, including a discussion of sparse-array beamforming that discloses the true broadband nature of the beamformer. Then, the general approach to minimum-energy adaptation is discussed, including the role of spatial smoothing and noise augmentation in enabling effective adaptation without time-averaging. Both element- and beam-based algorithms are described. Next, methods of implementing spatial smoothing are described, followed by comments about the use of a frequency-averaged covariance matrix. Two approaches to applying ALMA beamforming to long line arrays are described, followed by a discussion of the feasibility of applying the approach to other array shapes. The report concludes with a discussion of the relationship between the mixer output and the output of a replica correlator, and the methodology of extending the ALMA beamforming approach to replica-correlator-processed signals, including more general waveform types.

LFM MIXER PREPROCESSING

Consider an LFM signal of duration T and bandwidth B transmitted from a point source, reflected from a field of stationary point scatterers and received on an array of N identical point receivers located at positions $\vec{x}_n$. The scatterers are assumed to be far enough from the receiving array for their echoes to be treated as plane waves. The continuous time series received by each receiving element is broken up into a succession of windows of duration T with arbitrary overlap. The windows are processed independently and sequentially until all time delays of interest are processed. The process to be described for a typical window will match to every time-delay-resolution cell to be processed and to every direction hypothesis of interest, and will optimize the beamforming weights for each such combination. The window will be assumed to start at time t_0 and the parameters needed to match to an arbitrary resolution cell and direction will be derived by assuming that a point target signal arrives at time t_1 between t_0 and $t_0 + T$. The transmitted signal is represented in complex analytic form by

$$r(t) = e^{i\omega_0(1+at)t} \quad , \tag{1}$$

where

$$a = \frac{B}{2f_0T} \quad , \tag{2}$$

and

$$f_0 = \frac{\omega_0}{2\pi} \tag{3}$$

is the frequency at the beginning of the sweep. The assumed arrival time will be referenced to the beginning of the element-0 window. Let the shifted element-0 arrival time be defined by

$$\tau_0 = t_1 - t_0 \quad , \tag{4}$$

and let the assumed arrival direction be defined by a vector with magnitude ω_0/c. Then the arrival time of the signal at the n-th element may be obtained in terms of the projections of the element position vectors on the steering-direction axis as

$$\tau_n = \tau_0 - \frac{1}{\omega_0}\vec{u} \cdot (\vec{x}_n - \vec{x}_0) \quad . \tag{5}$$

The point-target signal arriving at the n-th element is represented (normalized to unit amplitude) by a delayed version of the transmitted signal as

$$g_n(t) = e^{i\omega_0[1+a(t-\tau_n)](t-\tau_n)} \quad . \tag{6}$$

The target signal is mixed with the replica to give

$$z_n(t) = r(t)g_n^*(t) = e^{i\omega_0[2a\tau_n t + \tau_n(1-a\tau_n)]} \quad , \tag{7}$$

where * denotes complex conjugate. Note that the mixer-output target response has a frequency

$$f(\tau) = 2af_0\tau \tag{8}$$

that is proportional to the time delay, and a phase term

$$\phi(\tau) = \omega_0\tau(1-a\tau) \tag{9}$$

that is to first order proportional to the time delay, but contains a small term quadratic in the time delay.

CONVENTIONAL BEAMFORMING AT THE MIXER OUTPUT

The process of beamforming for each assumed target delay and direction involves adjusting each element output by the frequency and phase shifts necessary to match all the elements to the same assumed target parameters. The required frequency shift to match the n-th element to the 0-th element is

$$\delta f_n = 2a\omega_0(\tau_0 - \tau_n) = 2a\vec{u} \cdot (\vec{x}_n - \vec{x}_0) \quad , \tag{10}$$

and the required phase shift is

$$\delta\phi_n = \omega_0[\tau_0(1-a\tau_0) - \tau_n(1-a\tau_n)] \quad . \tag{11}$$

The quadratic terms in eq. (11) are often small, and will be neglected for brevity in the present analysis, giving

$$\delta\phi_n = \omega_0(\tau_0 - \tau_n) = \vec{u} \cdot (\vec{x}_n - \vec{x}_0) \quad . \tag{12}$$

The conventional mixer beamformer matches all the element signals using the frequency and phase shifts given in eqs. (10) and (12), and sums them. The mixer output is first fast Fourier transformed (FFT) with a time window of length T. Note that the frequency resolution of the FFT is $1/T$. From eqs. (2) and (8) the time resolution corresponding to this frequency resolution is

$$\Delta t = \frac{\Delta f}{2af_0} = \frac{1}{B} \quad , \tag{13}$$

so the temporal resolution of the mixer process is the same as would be obtained from a matched filter. The resulting vector of element responses for the i-th frequency cell may be represented by

$$V_0 = \begin{bmatrix} v_0^{(0)}(f_i) \\ v_1^{(0)}(f_i) \\ \vdots \\ v_{N-1}^{(0)}(f_i) \end{bmatrix} \quad . \tag{14}$$

A steering direction is chosen and the frequency shifts are applied to obtain the shifted element response vector

$$V = \begin{bmatrix} v_0(f_i) \\ v_1(f_i) \\ \vdots \\ v_{N-1}(f_i) \end{bmatrix} = \begin{bmatrix} v_0^{(0)}(f_i - \delta f_0) \\ v_1^{(0)}(f_i - \delta f_1) \\ \vdots \\ v_{n-1}^{(0)}(f_i - \delta f_{N-1}) \end{bmatrix} \quad . \tag{15}$$

The shifted frequencies are rounded to the discrete FFT samples. The frequency shifts correspond, in the time domain, to the bulk time delays required to align the element time series so that the correlation peak of a point target falls in the same time-resolution cell at all the elements.

The shifted signals are then aligned within each resolution cell by applying a phase shift given by eq. (12). Without loss of generality, the constant term is dropped from the phase shifts, and a steering vector is defined by

$$S = \begin{bmatrix} e^{i\vec{u}\cdot\vec{x}_0} \\ e^{i\vec{u}\cdot\vec{x}_1} \\ \vdots \\ e^{i\vec{u}\cdot\vec{x}_{N-1}} \end{bmatrix} \quad . \tag{16}$$

The phase shifts are applied to the element responses to give the beamformed amplitude output as

$$A = S^H V \quad , \tag{17}$$

where H denotes conjugate transpose, and vectors and matrices are distinguished by bold type. The beamformed power is given by

$$P = AA^* = S^H V V^H S \quad . \tag{18}$$

In terms of the covariance (cross-spectral) matrix

$$C = VV^H \quad , \tag{19}$$

the output power for the conventional mixer beamformer is written

$$P = S^H C S \quad . \tag{20}$$

The properties of the conventional mixer beamformer will now be demonstrated through the results of simulations. In the simulations a 19-element line array was used with elements equally spaced at 0.49 wavelength at the frequency at the top of the FM sweep $f_0 + B$. The bandwidth was taken to be $f_0/10$, so that the length of the array was 1.76 times the range-resolution cell

width $c/(2B)$. These, incidentally, are the same parameters that were used in the simulations that produced figures 1 and 2. Two test scenarios are now defined:

> Scenario 1: Fifteen range-resolution cells are defined, the first being the closest to the array. The first and then every second cell contain a single 20-dB scatterer. The angular positions of the scatterers step counterclockwise in 20° increments beginning with the the first scatterer at 20° from broadside to the array.
>
> Scenario 2: Fifteen range-resolution cells are defined. In this case, the cell most distant from the array is designated as the first. Each cell contains two scatterers, one of which has a level of 23 dB, and the other has a lower level. The lower level scatterer has a level of 10 dB in the first range cell. In the succeeding range cells, the level of the lower level scatterer decreases in 3-dB steps. The angular positions of the 23-dB scatterers begin at 1° and step counterclockwise in 1° increments. The angular positions of the lower level scatterers begin at 10° and step counterclockwise in 5° increments.

The first scenario was designed to test the conventional and adaptive beamformer performance against well-range-separated large scatterers, while the second scenario was designed to test the ability to detect weak scatterers in the same range cell as strong ones. Figure 3(a) depicts the beamformer response versus steering angle to the scatterer in the first range cell in scenario 1. Figure 3(b) depicts the actual direction and amplitude of the scatterer. To test whether the response for the first range cell was affected by the presence of scatterers in the other cells, a response was produced with only the one range cell defined, and there was no visible difference in the resulting plot.

Figure 4(a) shows the response to the two scatters in the most distant range cell in scenario 2. Figure 4(b) depicts the two scatters with levels of 23 and 10 dB, respectively, in that cell.

The presence of the weaker scatterer is evidenced in what appears to be an enhanced level of the first sidelobe on the side of the mainlobe where the scatterer is. Note from figure 3 that the single-scatterer sidelobe level at the relative position of the 10-dB scatterer is about 13 dB below the mainlobe, or about equal to the 10-dB scatterer level.

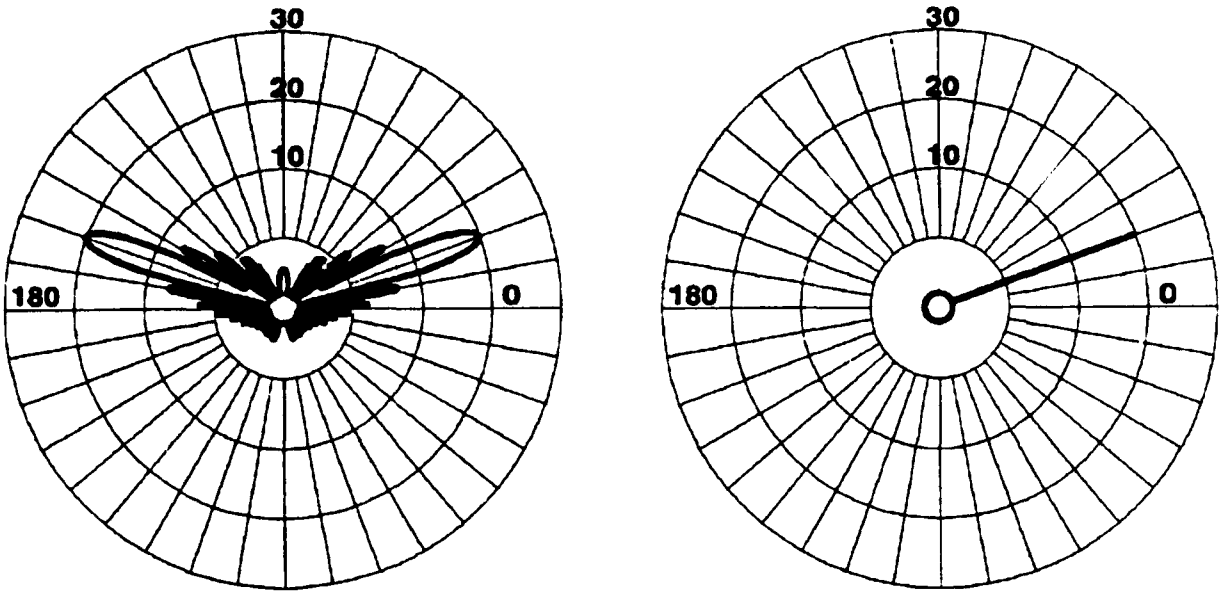

(a) (b)

Figure 3. (a) Conventional mixer beamformer response to a single-range cell from scenario 1. (b) Scatterer distribution in the range cell.

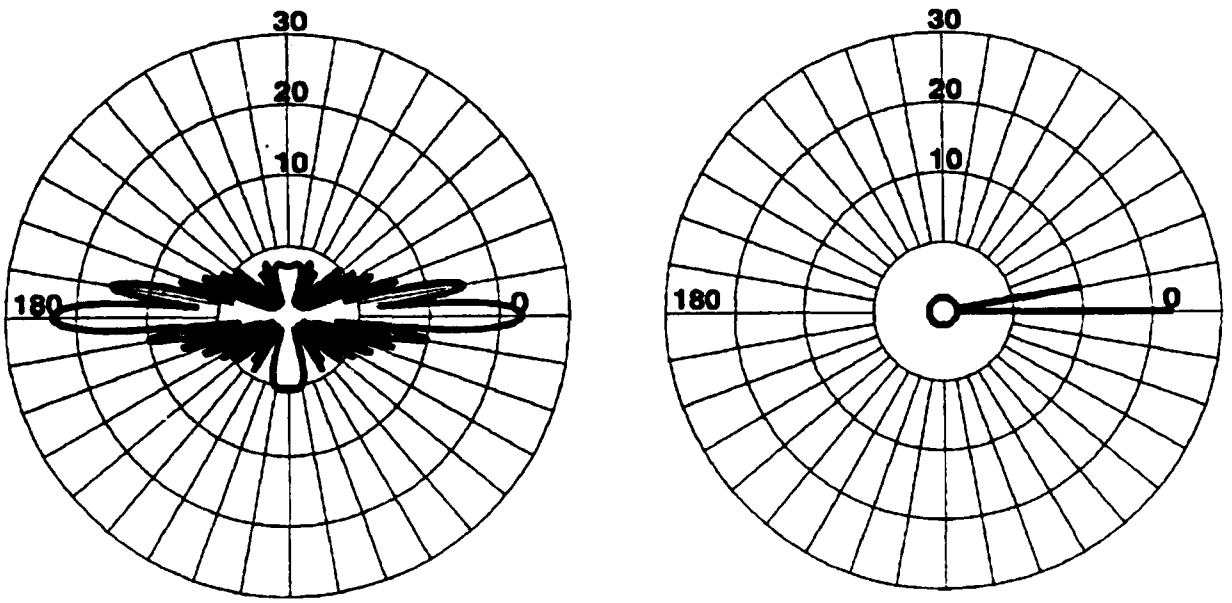

(a) (b)

Figure 4. (a) Conventional mixer beamformer response to a single-range cell from scenario 2. (b) Scatterer distribution in the range cell.

SPARSE-ARRAY RESPONSE OF THE CONVENTIONAL MIXER BEAMFORMER

It is noteworthy that the LFM mixer beamformer is truly a broadband beamformer. The type of broadband results that are typically obtained by Fourier synthesis of frequency-sampled narrowband results are produced directly. The LFM mixer has the property that most of the echo energy from a point target is compressed to a time interval of approximately the inverse of the bandwidth. This property is shared by many other useful waveform processes such as matched-filtered HFM, cw pulses, and impulsive waveforms. For waveforms having this property, the LFM mixer beamformer simulator can be used to model their approximate beamformer performance. For example, the performance of an approach proposed by Huster, Miklovic, and Schmidt (1993) that involves receiving broadband signals on a sparse array can be simulated. To demonstrate the results of such a simulation, the same scenarios are used. The array is made sparse by increasing the element spacing by a factor of 10, and the signal is made ultrawide-band by increasing the bandwidth by a factor of 8. The two scenarios occupy a much shorter range interval than before because of the reduced range-cell width due to the wider bandwidth. Figure 5 shows the response of the mixer beamformer for the sparse array, broadband case against a single point target that is the one from scenario 1 depicted in figure 3(b). In this case, however, only the single scatterer was present; the rest of the scenario was not defined. As indicated by Huster et al. (1993), the response consists of a narrow mainlobe and a constant pedestal at a level below the mainlobe of 20log N, where the number of elements is in the array. What has occurred is that the demodulated echo is effectively a very short pulse; except when the array is steered at the target, only one element receives the echo at any one time. Hence, the pedestal is actually the single-sensor-response level.

When the whole scenario 1 is defined, the single-range-cell response changes drastically as shown in figure 6. Now, when the array is not steered at the target in the range cell of interest, it receives a superposition of all the scatterers in the scenario that happen to come in at the same time. This observation, which was not reported by Huster et al. (1993), suggests that sparse-array beamforming may not be well suited to a high-clutter environment such as the shallow-water environment for which it was proposed.

Another example of sparse-array beamforming has been simulated for scenario 2. With only the range cell depicted in figure 4(b) defined, the response images the distribution well, as shown in figure 7. However, when the whole scenario is defined, the result for the same range cell is as shown in figure 8. Not only do the high sidelobes make it practically impossible to detect the presence of the weaker target, the level of the larger target has been substantially augmented by the signals in the other range cells.

The LFM mixer compresses the broadband LFM pulse and maps the arrival time of the compressed-pulse event into frequency space. The amplitudes and phases of the mixer-output spectrum were conventionally beamformed using the equivalent of narrowband beamforming methods; yet the results are truly broadband. The method of adaptively beamforming the mixer outputs by methods that are formally similar to narrowband ABF techniques will now be presented.

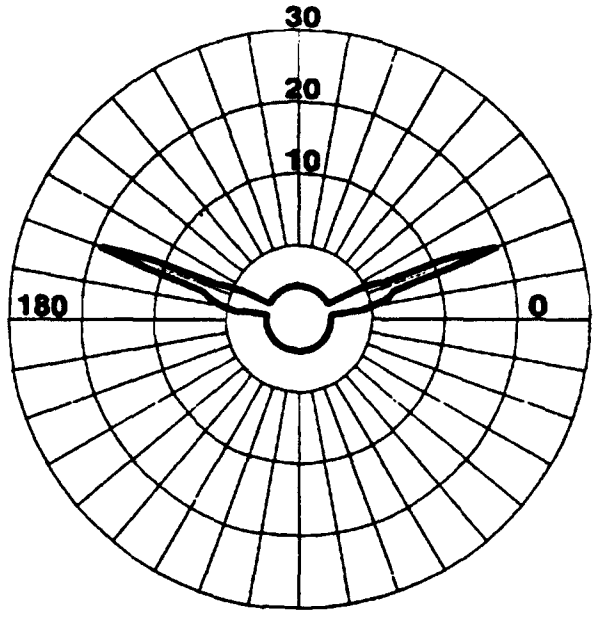

Figure 5. Sparse-array response for scenario 1 with only one-range cell defined.

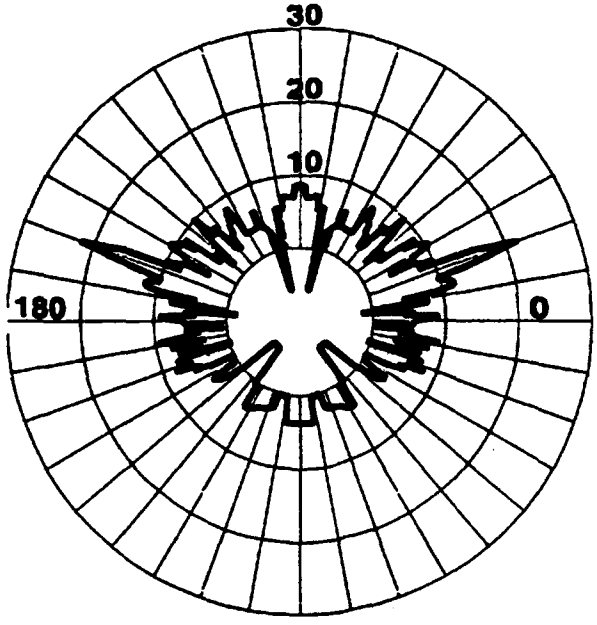

Figure 6. Sparse-array response for one-range cell from scenario 1 with entire scenario defined.

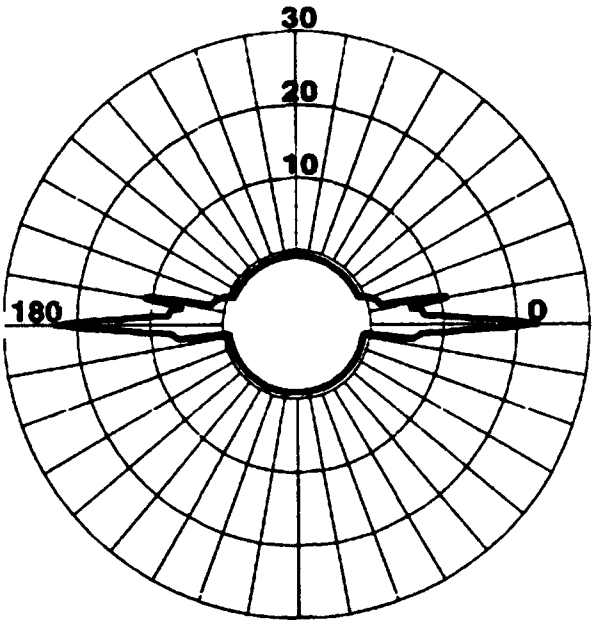

Figure 7. Sparse-array response for scenario 2 with only one-range cell defined.

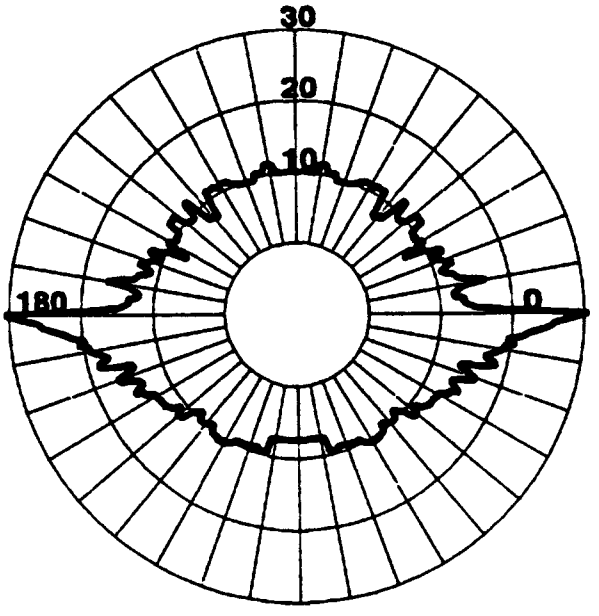

Figure 8. Sparse-array response for one-range cell from scenario 2 with entire scenario defined.

ELEMENT-BASED MINIMUM-ENERGY ADAPTATION

The adaptive processing approach used in ALMA beamforming is formally similar to the constrained minimum-energy type of adaptation that is well known in the passive signal-processing literature. Different variants of the ALMA algorithm have been developed, based on both element-based and beam-based adaptation. The element-based approach will be described first. A general discussion of this type of algorithm can be found in an article by Cox, Zeskind, and Owen (1987). As in the case of passive ABF, optimal weights are derived subject to one or more directional gain constraints. In the present approach, a weight vector W is derived that minimizes the array output power

$$P_{ME} = W^H C W \quad , \tag{21}$$

subject to the constraint that the signal gain in the direction to which the array ed be unity

$$W^H S = 1 \quad . \tag{22}$$

Assuming that a suitable average covariance can be estimated, the optimum weight solution is of the form found in Cox et al. (1987).

$$W = \frac{\overline{C}^{-1} S}{S^H \overline{C}^{-1} S} \quad . \tag{23}$$

SPATIAL SMOOTHING

In passive ABF, the average *covariance* is normally taken to be the ensemble average of a long-term stationary noise process. Under the assumption of uncorrelated signals and noise, the weights preserve any signal that is precisely matched to a constraint and tend to null other, interfering signals.

Some approaches to active ABF apply the same passive approach and adapt against discrete passive noise sources. While such an approach is beneficial in an environment in which detection is limited by passive interferers, it is not expected to be effective against reverberant features because reverberation does not typically remain stationary long enough for a useful ensemble average covariance to be acquired.

Obtaining an average covariance that leads to weights that are effective against reverberant features, without suppressing signals, is the fundamental problem in active adaptive beamforming. In ALMA beamforming, the weights are derived for each time-resolution cell independently, with no time-averaging. Rather than time averaging, "spatial-smoothing," based on the approach detailed in an article by Shan and Kailath (1985), is used to build up as much independent signal and noise information as possible. Briefly, this approach involves averaging the sample covariances of some number of highly overlapped subarrays. The details of forming the spatially smoothed covariances are given in a later section of this report. Spatial-smoothing was developed to overcome signal suppression problems in passive ABF due to correlated signals and interference. Signal suppression occurs in active ABF due to the fact that all signals and interference within a single time-resolution cell are correlated.

NOISE AUGMENTATION

According to Shan and Kailath (1985), the maximum number of discrete, correlated signals against which spatial-smoothing is effective is equal to the number of subarrays. It cannot generally be guaranteed in the "single-snapshot" adaptation implemented in ALMA that the number of correlated signals will not exceed the number of subarrays. Moreover, the signal-snapshot covariance does not contain any uncorrelated signals or noise. These considerations lead to the requirement for augmentation of the main diagonal of the average covariance estimate to take the place of the noise that occurs naturally in the passive problem. This "pseudonoise" is present in the covariance only for the purpose of weight calculation. The weights are then applied to the original data. The pseudonoise performs two important functions. First, it improves the solution in cases where there are too many signals to be handled by the number of subarrays, by effectively masking all but the strongest signals. Second, it improves the ability to estimate the signal and interference levels by reducing the sensitivity to errors. In the latter role, pseudonoise is similar to the white-noise-gain constraint discussed by Cox et al. (1987). It is also equivalent to "ridge regression" discussed by Hoerl and Kennard (1970). The effects of noise augmentation on passive ABF performance were explored in an unpublished report by Lockwood (1986)*. Lockwood's analysis was based on an idea found in a report by Medoff et al. (1985). The process of noise augmentation as used in the present work is now described. Let $\overline{C}_s$ represent the average covariance prior to noise augmentation. Then the noise-augmented average covariance is given by

$$\overline{C} = \overline{C_s} + f_n N \bar{p}_e I \ , \tag{24}$$

where $\bar{p}_e$ is the average element power, N is the dimension of the covariance matrix and f_n is a numeric parameter, which, for the following simulations, as well as for the results presented in figure 2, was taken equal to 0.09 and I is an identity matrix. It is emphasized that the noise-augmented average covariance is used only for the adaptive weight calculation. The single-sample covariance is used in eq. (21) to compute the beamformer output power.

ELEMENT-BASED MINIMUM-ENERGY ADAPTATION SIMULATION RESULTS

Before presenting the results of combining both spatial-smoothing and noise augmentation, results of using noise augmentation alone will be presented to help clarify the role of each of the two techniques. As will be seen in a later section, the covariance of only a single subarray is just the outer product of its response vector with the Hermitian transpose of the response vector. The covariance is, therefore, singular, and cannot be inverted. Noise augmentation allows an otherwise singular, or nearly singular matrix to be inverted. Figure 9 shows the adaptive response to the scenario 1 scatterer depicted in figure 3(b), when noise augmentation is used. It is evident that the scatterer is well imaged by the algorithm, despite the singular nature of the original covariance matrix. This is the principal need for noise augmentation, and this example underscores the equivalence of the present use of noise augmentation and ridge regression as described in by Hoerl and Kennard (1970).

---

* Technical Notes (TNs) are working documents and do not represent an official policy statement of the Naval Command, Control and Ocean Surveillance Center, RDT&E Division. For further information, contact the author.

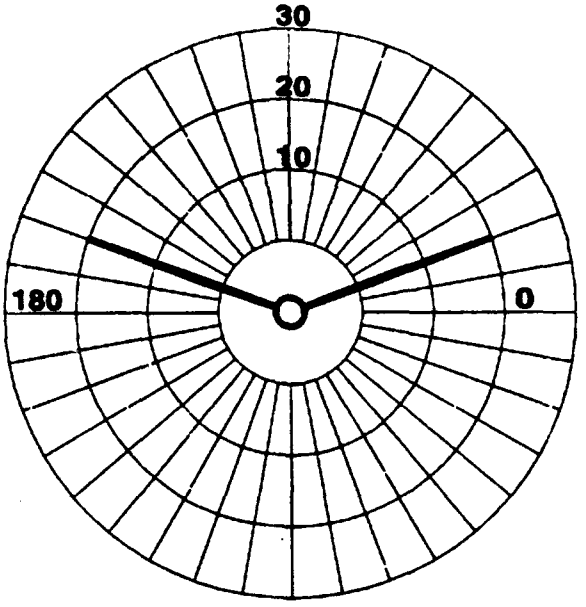

Figure 9. Adaptive response to one-range cell from scenario 1.

Figure 10 demonstrates the need for spatial-smoothing. This figure shows the adaptive response to the scenario 2 scatterers depicted in figure 4(b). It is seen that only the stronger of the two scatterers is imaged, and at greatly reduced level. Because the two scatterer signals are correlated, they cancel each other when the adaptive algorithm is applied. This effect is similar to what happens in passive ABF when correlated multipath signals are encountered, which is the problem addressed by Shan and Kailath (1985).

The addition of spatial-smoothing permits the imaging of multiple (correlated) signals within a single range-resolution cell. The number of signals that can be handled is theoretically equal to the number of subarrays. In the example that will now be described, as well as in the result presented in figure 2, 11 19-element subarrays were simulated. The total number of elements on the subarray was 29. Rather than show the result of spatial-smoothing for the same range cell from scenario 2 that was used in the foregoing results, a range cell was chosen wherein the weaker scatterer was so weak as not to be detectable at all in the conventional response. The conventional response for this particular range cell is shown in figure 11, and the true scatterer distribution is shown in figure 12.

The adaptive result presented in figure 13 shows that the weak as well as the strong scatterer have been imaged well.

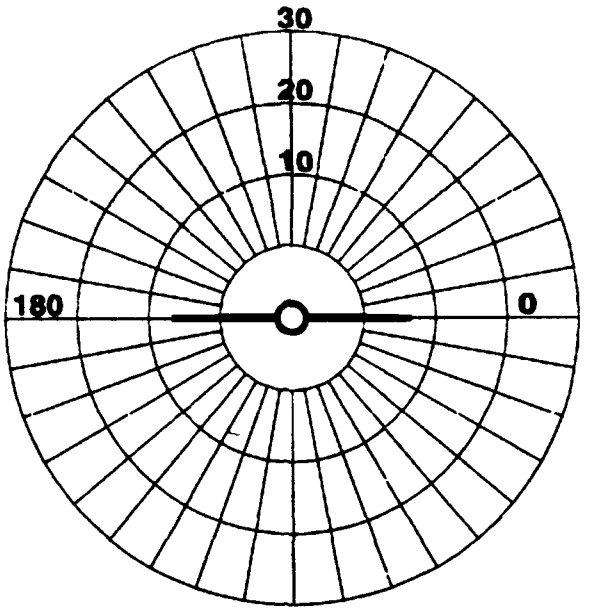

Figure 10. Adaptive response to one-range cell from scenario 2: noise augmentation, but no spatial-smoothing.

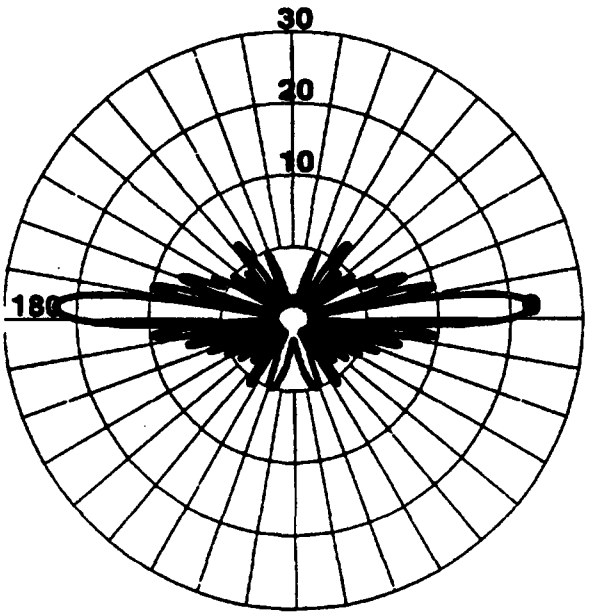

Figure 11. Conventional response to scenario 2 range cell with the weaker scatterer at 1-dB level.

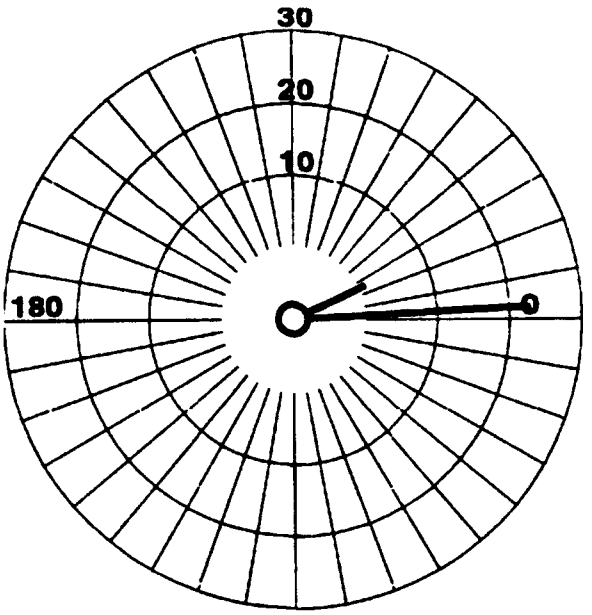

Figure 12. Scenario 2 range cell scatterer distribution showing direction and magnitude of 23- and 1-dB scatterers.

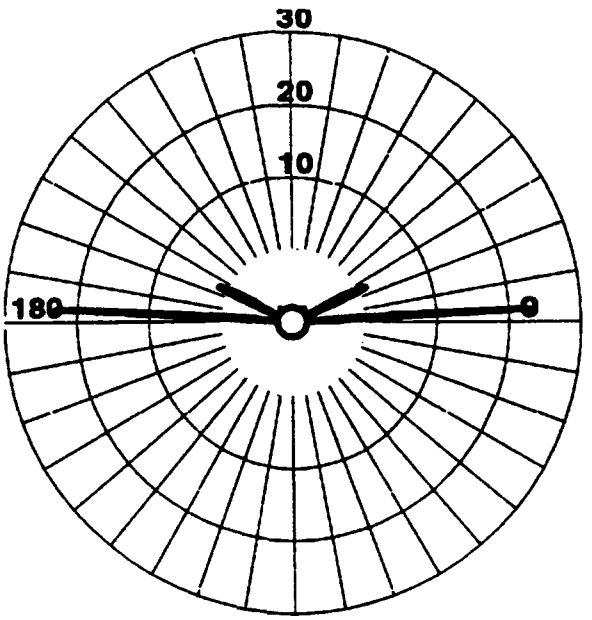

Figure 13. Adaptive response with spatial-smoothing, to scenario 2 range cell with the weaker scatterer at 1-dB.

It is pointed out that the adaptive algorithm with spatial-smoothing does not always perform in the ideal fashion demonstrated here. Problems can arise from the fact that the signals are limited in time; so, the interference field affecting one subarray is not generally quite the same as that affecting the others. These differences among the subarrays can lead to signal suppression, and the effect tends to get worse as the number of subarrays becomes large. Also, as may be seen from figure 2, the effectiveness of spatial-smoothing in eliminating signal suppression tends to be degraded near endfire to the line array. These effects, which can degrade the performance of ALMA beamforming, are minimized by noise augmentation. There is a tradeoff in the amount of noise augmentation to use between signal suppression if too little is used and inadequate sidelobe suppression if too much is used.

BEAM-BASED MINIMUM-ENERGY ADAPTATION

In addition to the element-based approach, a variant of ALMA beamforming has been implemented using constrained beam-based minimum energy adaptive processing. The algorithm follows an approach outlined by Vural (1975) for narrowband passive beamforming. A beamforming matrix F transforms the $N \times N$ element-based covariance C into a $K \times K$ beam-based covariance

$$B = F^H C F \quad , \tag{25}$$

where K is the number of beams that are to be combined in a weighted sum to produce the adaptive beamformer output. The steering vector for the constraint direction is transformed to the beam-space direction vector by

$$D = F^H S \quad , \tag{26}$$

which is a vector of beamformed responses, to a unit plane-wave signal from the direction associated with S, for each of the K beam-steering directions. Weights are then sought that minimize the array output power

$$P_{ME} = W^H B W \quad , \tag{27}$$

subject to the constraint

$$W^H D = 1 \quad . \tag{28}$$

As in the element-based case, assuming a suitable average covariance can be estimated, the solution for the weights is as stated in by Vural (1975)

$$W = \frac{\bar{B}^{-1} D}{D^H \bar{B}^{-1} D} \quad . \tag{29}$$

The way the beam-based covariance is defined in the present work differs from the passive formulation in that the beam outputs embodied in the covariance matrix are not, in general, the same as the outputs that would be obtained if beams were actually steered in those directions. The reason is that, prior to forming the covariance matrix, the element responses are adjusted to compensate for the bulk time-delay differences among the elements for a specific steering direction. In the present work, the beam associated with that steering direction is always indexed the first, and the remaining beams, which are transformations of the same element data, are indexed in the order of increasing angular distance from the first.

The way the beam directions have been chosen in the present work has been to first divide the available steering cosine space into N equal increments, beginning with the steering direction to be calculated. (Any additional directions would contain redundant information.) The beams are then ordered by proximity to the steering direction, and the first $K \leq N$ are selected.

The means employed to obtain the spatially smoothed average beam-based covariance are discussed in a subsequent section.

SPATIALLY AVERAGED ELEMENT AND BEAM COVARIANCE

The spatially averaged element and beam covariances are now derived. Because of the frequency-domain nature of this analysis, the outer products of element response vectors that are referred to herein as covariance matrices might more properly be referred to as cross-spectral matrices; nevertheless, the term covariances will be used. The average covariances will be formed from the sample covariances of some number M of highly overlapped subarrays, each having N elements. The beam covariances will be defined as transformations of the element covariances using the steering vectors appropriate to some arbitrary set of independent beam directions. Because of the nonstationarity of the active sonar scenario, the beam responses embodied in the beam covariances do not necessarily correspond to the responses that would be obtained if beams were actually steered in the set of beam directions. Rather, the beam covariances should be thought of linear transformations of the element-covariance data, where the element responses have been adjusted by the appropriate time delays for one specific look direction.

Let the steering vector for subarray *0 steered* to the look direction be

$$S_0 = \begin{bmatrix} s_0 \\ s_1 \\ \vdots \\ s_{N-1} \end{bmatrix} , \tag{30}$$

and let the corresponding steering vector for subarray m be

$$S_m = \begin{bmatrix} s_m \\ s_{m+1} \\ \vdots \\ s_{N-1+m} \end{bmatrix} , \tag{31}$$

where the steering vector component for the n-th element is given by

$$s_n = e^{i\vec{u}\cdot\vec{x}_n} . \tag{32}$$

The steering vector for the m-th subarray may be rewritten in terms of the components of the 0-th subarray steering vector as

$$S_m = \begin{bmatrix} (s_m s_0^*)s_0 \\ (s_{m+1} s_1^*)s_1 \\ \vdots \\ (s_{N-1+m} s_{N-1}^*)s_{N-1} \end{bmatrix} , \tag{33}$$

which may be rewritten as the product of a diagonal matrix and S_0

$$S_m = \begin{bmatrix} s_m s_0^* & & & \\ & s_{m+1} s_1^* & & 0 \\ & & \ddots & \ddots \\ 0 & & & s_{m+N-1} s_{N-1}^* \end{bmatrix} S_0 \quad . \tag{34}$$

Let

$$\Delta_m = \begin{bmatrix} s_m & & & \\ & s_{m+1} & & 0 \\ & & \ddots & \\ 0 & & & s_{m+N-1} \end{bmatrix} \quad , \tag{35}$$

so that

$$S_m = \Delta_m \Delta_0^H S_0 \quad . \tag{36}$$

In the special case of an equally spaced (periodic) line array,

$$\Delta_m \Delta_0^* = e^{i\vec{u} \cdot (\vec{x}_m - \vec{x}_0) I} \quad , \tag{37}$$

so that S_m is equal to a scalar times S_0

$$S_m = e^{i\vec{u} \cdot (\vec{x}_m - \vec{x}_0)} S_0 \quad . \tag{38}$$

In forming an element-based covariance matrix averaged over subarrays, it is generally necessary to weight each subarray sample covariance so that the same steering vector can be used for all samples to form a beam in a given steering direction. The M subarray covariances will now be transformed to use the subarray-0 steering vector using the foregoing relationships. The conventional beam response of the m-th subarray in the desired steering direction is given by

$$P_m = S_m^H C_m S_m \quad , \tag{39}$$

which may be rewritten in terms of the subarray-0 steering vector using eq. (36) as

$$P_m = S_0^H \Delta_0 \Delta_m^H C_m \Delta_m \Delta_0^H S_0 \quad . \tag{40}$$

Note that in the special case of a periodic line array, eq. (38) applies, and the m-th subarray beam response reduces to

$$P_m = S_0^H C_m S_0 \quad . \tag{41}$$

The average covariance $\overline{C}$ of the M subarrays is now defined by

$$\overline{C} = \frac{1}{M} \sum_{m=0}^{M-1} \Delta_0 \Delta_m^H C_m \Delta_m \Delta_0^H \quad , \tag{42}$$

so that the average beam response can be written in terms of the subarray-0 steering vector as

$$\overline{P} = \frac{1}{M}\sum_{m=0}^{M-1} P_m = S_0^H \overline{C} S_0 \quad . \tag{43}$$

For the special case of the periodic line array, it follows from eq. (41) that the average covariance may be written

$$\overline{C} = \frac{1}{M}\sum_{m=0}^{M-1} C_m \quad . \tag{44}$$

To convert to a beam-based covariance, K beam steering directions denoted by θ_k are defined with the steering vector of the m-th subarray steered to the k-th steering direction denoted by S_{mk}. Then the beam-based covariance of the m-th subarray is

$$B_m = F_m^H C_m F_m \quad , \tag{45}$$

where

$$F_m = \left(S_{m0}\ S_{m1}\ \cdots\ \cdots\ S_{m(K-1)}\right) \tag{46}$$

is the transformation matrix, each column of which contains one of the K steering vectors. We require a beam-based covariance averaged over the subarrays that is related to the element-based average covariance by a transformation of the form of eqs. (45) and (46). In general, such an average is not simply obtained as a weighted sum of the B_m. Therefore, the approach of defining the average beam-based covariance by transforming $\overline{C}$ using F_0 has been adopted. This transformation gives

$$\overline{B} = F_0^H \overline{C} F_0 \quad . \tag{47}$$

In the special case of a periodic line array, the average beam-based covariance defined by eq. (47) can be written in terms of the subarray beam-based covariances. It follows from eq. (38) that the steering vector for the k-th direction may, in this case, be written

$$S_{mk} = e^{i\vec{u}_k \cdot (\vec{x}_m - \vec{x}_0)} S_{0k} \quad . \tag{48}$$

Then, eq. (46) may be rewritten

$$F_m = \left(e^{i\vec{u}_0 \cdot (\vec{x}_m - \vec{x}_0)} S_{00}\ e^{i\vec{u}_1 \cdot (\vec{x}_m - \vec{x}_0)} S_{01}\ \cdots\ \cdots\ e^{i\vec{u}_{(K-1)} \cdot (\vec{x}_m - \vec{x}_0)} S_{0(K-1)}\right) . \tag{49}$$

Let

$$D_m = \begin{bmatrix} e^{i\vec{u}_0(\vec{x}_m - \vec{x}_0)} & & & \\ & e^{i\vec{u}_1(\vec{x}_m - \vec{x}_0)} & & 0 \\ & & \ddots & \\ 0 & & & \ddots \\ & & & e^{i\vec{u}_{(K-1)} \cdot (\vec{x}_m - \vec{x}_0)} \end{bmatrix} . \tag{50}$$

Then, for the periodic line array,

$$F_m = F_0 D_m \quad . \tag{51}$$

Note that D_m has the property that

$$D_m^H = D_m^{-1} \quad . \tag{52}$$

From eqs. (45), (51), and (52), it follows that

$$D_m B_m D_m^{-1} = F_0^H C_m F_0 \quad . \tag{53}$$

Equations (44), (47), and (53) then lead to an expression for the average beam-based covariance in terms of the subarray beam-based covariances for the special case of a periodic line array

$$\overline{B} = \frac{1}{M} \sum_{m=0}^{M-1} D_m B_m D_m^{-1} \quad . \tag{54}$$

SPATIAL SMOOTHING WITH SINGLE-ELEMENT SHIFTS

It is often advantageous to implement spatial-smoothing with the successive subarrays offset by only one element. In that case, it will be seen that the subarray-averaging is equivalent to averaging along the diagonals of a suitably transformed covariance matrix. Consider an array of N_T elements with element responses v_n. A weighted response will be defined by

$$u_n = s_n^* v_n \quad , \tag{55}$$

which may be regarded as the components of the $N_T \times 1$ response vector U. A transformed covariance matrix for the entire array may be defined by

$$C_T' = UU^H \quad . \tag{56}$$

If N-element subarrays are to be defined with the 0-th subarray starting with the 0-th element and extending to the $(N-1)$-th element and the m-th subarray starting with the m-th element and extending to the $(N+m-1)$-th element, then the weighted covariance matrix C_m' of the m-th subarray is a submatrix of C_T' extending from the m-th row to the $(N+m-1)$-th row and from the m-th column to the $(N+m-1)$-th column. Note that the subarray covariance matrices are diagonally displaced from each other. The components of C_m' are

$$c_{ij}^{'(m)} = u_{m+i} u_{m+j}^* = s_{m+i}^* v_{m+i} v_{m+j}^* s_{m+j} \quad , \tag{57}$$

which are equivalent to the components of $\Delta_m^H C_m \Delta_m$. Therefore, the weighted covariance matrix may be written

$$C_m' = \Delta_m^H C_m \Delta_m \quad , \tag{58}$$

and the average covariance as given by eq. (42) may be rewritten

$$\overline{C} = \Delta_0 \left\{ \frac{1}{M} \sum_{m=0}^{M-1} C_m' \right\} \Delta_0^H \quad . \tag{59}$$

SUMMATION ALONG DIAGONALS

Since the C'_m are submatrices of C'_T displaced diagonally from each other, it may be seen that the quantity in braces in eq. (59) can be obtained from C'_T by redefining an $N \times N$ submatrix in the upper left-hand corner, where each component is obtained by averaging along the diagonal running downward and to the right over M terms, beginning with the term in the position being calculated. The resulting matrix is then pre and postmultiplied by Δ_0 and its transpose, respectively, to give $\overline{C}$. The result of the operations just described may be represented in component form as

$$\overline{c_{ij}} = \frac{1}{M} \sum_{m=0}^{M-1} s_i c'_{(i+m)(j+m)} s_j^* \quad , \tag{60}$$

which may also be written

$$\overline{c_{ij}} = \frac{1}{M} \sum_{m=0}^{M-1} s_i u_{(i+m)} u_{(j+m)}^* s_j^* \quad . \tag{61}$$

DATA MATRIX REPRESENTATION

An alternative way of forming the average covariance, equivalent to the foregoing summation along diagonals, is by forming a data matrix consisting of the M weighted subarray response vectors arranged as columns

$$\mathrm{Y} = \begin{bmatrix} u_0 & u_1 & u_2 & \cdots & \cdots & u_{M-1} \\ u_1 & u_2 & u_3 & \cdots & \cdots & \vdots \\ u_2 & u_3 & \cdots & \cdots & \cdots & \vdots \\ \vdots & \vdots & \vdots & \vdots & \vdots & \vdots \\ u_{N-1} & u_N & u_{N+1} & \cdots & \cdots & u_{N+M-2} \end{bmatrix} \quad . \tag{62}$$

The average covariance can then be written

$$\overline{C} = \frac{1}{M} \Delta_0 \mathrm{Y} \mathrm{Y}^H \Delta_0^H \quad , \tag{63}$$

the components of which may be verified to be given by eq. (61).

In the case of a periodic-line array, the data matrix representation may be further simplified. In this case, by use of eqs. (38) and (55), it is seen that each row of υ must be multiplied by s_i^*, while each column must be multiplied by $e^{i\vec{u}\cdot(\vec{x}_j - \vec{x}_0)}$. Therefore, Y may be written as the product

$$\mathrm{Y} = \Delta_0^H \mathrm{N} \Psi^H \quad , \tag{64}$$

where

$$\Psi = \begin{bmatrix} 1 & & & \\ & e^{i\vec{u}\cdot(\vec{x}_1-\vec{x}_0)} & & 0 \\ & & \ddots & \\ 0 & & & e^{i\vec{u}\cdot(\vec{x}_{M-1}-\vec{x}_0)} \end{bmatrix} , \tag{65}$$

and

$$\mathrm{N} = \begin{bmatrix} v_0 & v_1 & v_2 & \cdots & \cdots & v_{M-1} \\ v_1 & v_2 & v_3 & \cdots & \cdots & \vdots \\ v_2 & v_3 & \cdots & \cdots & \cdots & \vdots \\ \vdots & \vdots & \vdots & \vdots & \vdots & \vdots \\ v_{N-1} & v_N & v_{N+1} & \cdots & \cdots & v_{N+M-2} \end{bmatrix} . \tag{66}$$

Equation (64) is now substituted into eq. (65), and it is observed that

$$\Delta_0 \Delta_0^H = I \quad , \tag{67}$$

and

$$\Psi_0 \Psi_0^H = I \quad . \tag{68}$$

Hence, the average element-based covariance for a periodic line array may be written

$$\overline{C} = \frac{1}{M} \mathrm{N}\mathrm{N}^H \quad . \tag{69}$$

BEAM COVARIANCE IN TERMS OF DATA MATRIX

Equation (61) may now be substituted into the definition of the beam-based average covariance given in eq. (47) to obtain

$$\overline{B} = \frac{1}{M} F_0^H \Delta_0 \mathrm{Y}\,\mathrm{Y}^H \Delta_0^H F_0 \quad . \tag{70}$$

By forming the products among F_0, Δ_0 and Y first, the $K \times K$ matrix $\overline{B}$ may be formed without first forming the $N \times N$ matrix $\overline{C}$. This may result in a significant computational savings if N is greater than K.

In the periodic line-array case, the computation of the beam-based covariance may be further simplified by use of eq. (69) . The equivalent expression for that case may be written

$$\overline{B} = \frac{1}{M} F_0^H \mathrm{N}\mathrm{N}^H F_0 \quad . \tag{71}$$

FREQUENCY-AVERAGED COVARIANCE

The idea of frequency averaging to obtain an invertible covariance is included here for completeness. The procedure would be to form the sample covariances for some number of frequencies, K, perhaps centered on the frequency cell to be beamformed f_i and then average them to form a nonsingular average covariance

$$\overline{C} = \frac{1}{K} \sum_{k=-K/2}^{K/2} C(f_{i+k}) \quad . \tag{72}$$

This approach effectively forms a matrix of the cross correlations of all the element pairs over the time spanned by the cells being averaged. Such a technique might be effective against random processes that were stationary over the group of cells, but this cannot generally be assumed to hold for active scatterers, and certainly does not hold for the point scatterers used to date in this work. Attempts to use frequency-averaging in simulations with point scatterers have led to that result, while the resulting average covariance is generally nonsingular, there is no significant improvement in the signal-suppression problem.

APPLICATION OF ALMA BEAMFORMING TO LONG ARRAYS

Methods of applying ALMA beamforming to long line arrays are now discussed. Fully adaptive solutions applied to long arrays are often impractical due to the large size of the covariance matrix that must be inverted. Even the 19×19 matrix inverted in the examples presented herein would require a super computer to process in realtime. Two methods of adapting long arrays have been implemented. The first is the beam-based solution, which lends itself especially well to long arrays. All the available elements are used to form the beams, but the matrix inversion is kept to a reasonable size by limiting the number of beams in the covariance. Because all of the signals and interferers are correlated, there seems to be no advantage to having more degrees of freedom than there are subarrays. It may, therefore, be argued that the number of beams and subarrays should be chosen to be equal. The number of subarrays is chosen based on the number of scatterers that need to be resolved in each range annulus, and is scenario-dependent. It has been observed that too many subarrays can be counter productive, increasing the tendency toward signal suppression. This appears to be caused by the fact that when subarrays are displaced from each other a distance of the order of the range resolution along the array, the fields of scatterers received by the corresponding elements at any given time are substantially different. Once the subarray fields are substantially different, they no longer contribute effectively to spatial-smoothing, for the same reason that frequency-averaging has been found to be ineffective.

A problem that has been observed in results of the beam-based ALMA algorithm applied to long arrays is that scatterers very close to each other in angle tend to suppress each other. It is believed that this effect is due to the fact that the ability of the long array to resolve individual scatterers exceeds the ability of the short distribution of subarray offsets to provide independent samples of the covariance.

The second approach to ALMA beamforming uses an element-based algorithm. The size of the covariance is reduced to a reasonable size by adapting the array in J segments. Each segment of N elements is adapted using spatial-smoothing over M subarrays and the weights are stored. The total number of elements thus used is

$$N_T = JN + M - 1 \quad . \tag{73}$$

Once all the segment weights have been calculated, a sum beam is formed using all but the last $M - 1$ elements. If one needed to use all the elements in the sum beam, one could form a segment from the last $M - 1$ elements and form subarrays displaced back toward the beginning of the array. This method of using the last elements has not yet been implemented. The segment adaptation method has the drawback that a short segment is limited by its inherent resolution in its ability to suppress sidelobes close to the main lobe of the high-resolution sum beam.

Within the limitations of the PC-based simulation program, results obtained using the two long-array algorithms are now compared with the fully adaptive, element-based algorithm. These simulations used parameters similar to the one presented at the beginning of this report (figure 2). However, the total number of elements was changed to 32 so that all three approaches could be directly compared using the same number of elements. The first result shown in figure 14 is the fully adaptive result with 11 22-element subarrays. This will be the standard against which the other faster approaches will be judged.

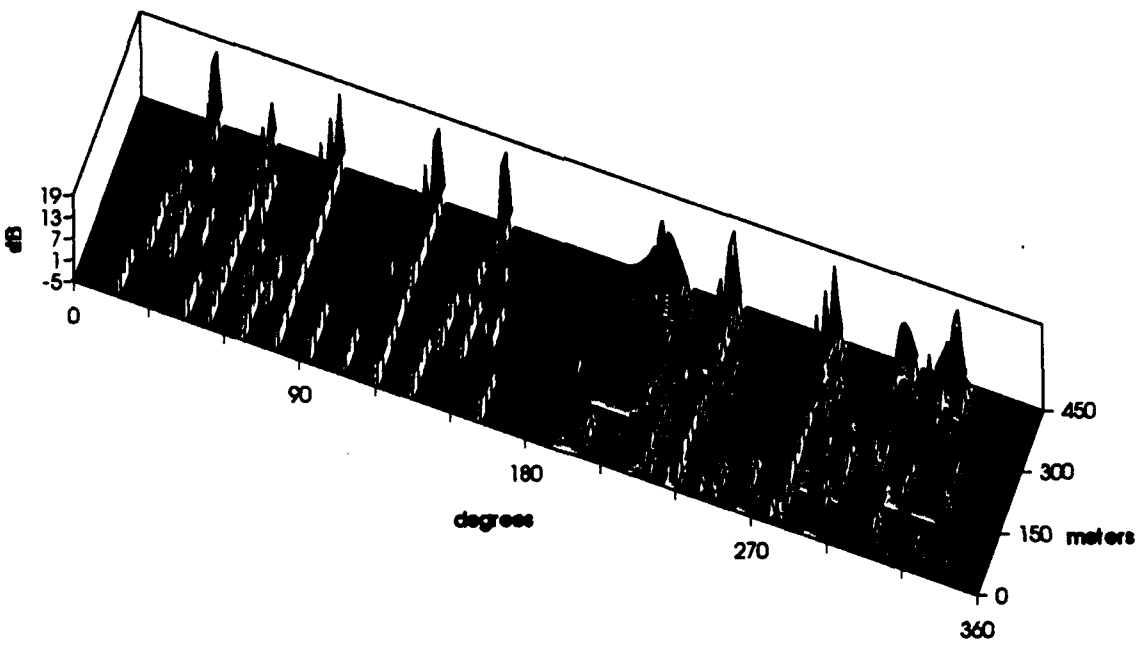

Figure 14. ALMA beamformer response to "ALMA" scatterer distribution for 22-element array, 11 subarrays.

The beam-based result is shown for comparison in figure 15. Here, 11 22-element beams were formed using 11 subarrays. The order of the covariance matrix that is inverted in the process is half that of the fully adaptive approach; so, in practice the algorithm should be of the order of 8 times faster. On can observe in the endfire regions (near 180 and 360 degrees) an increase in the sidelobe levels relative to the fully adaptive case, but otherwise the performance is comparable.

The other case consisted of element-based processing of two 11-element segments using 11 subarrays. The weights for each segment were derived and then a sum beam was formed using all 22 elements. It is noted in passing that weights could have been obtained for the last 10 elements by forming subarrays offset in the opposite direction, and all 32 elements could have been summed. The result of the simulation is shown in figure 16. The quality of the results is generally similar to the beam-based result, although the response peaks are not quite as sharp, and in some cases have a definite shoulder.

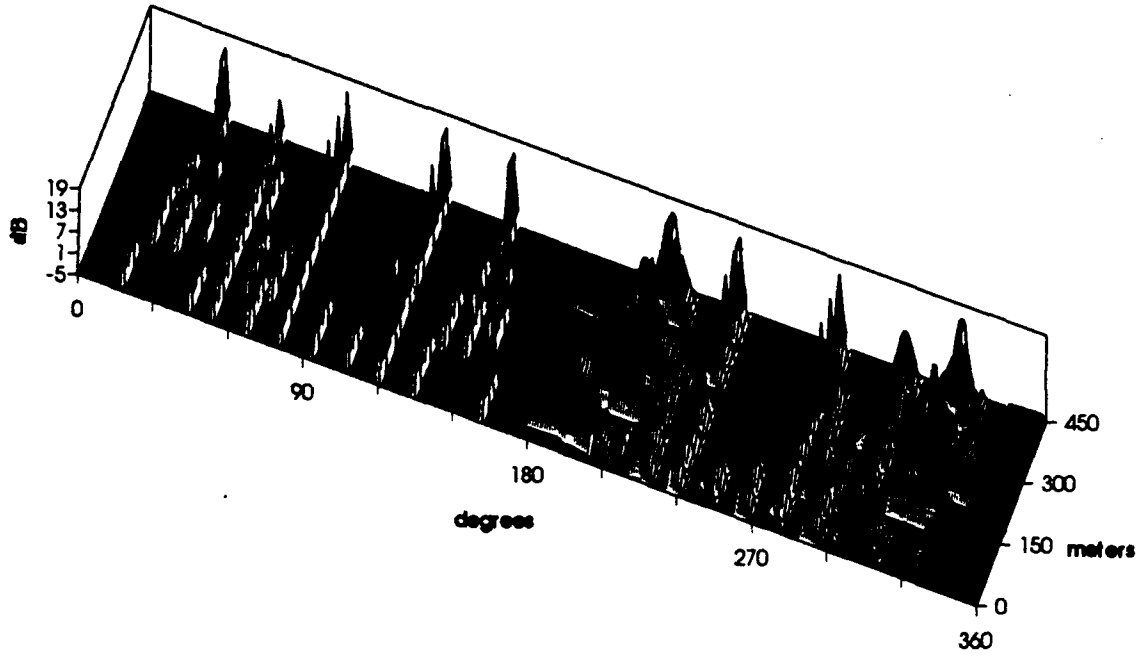

Figure 15. ALMA beamformer response to "ALMA" scatterer distribution for 11 22-element beams, 11 subarrays.

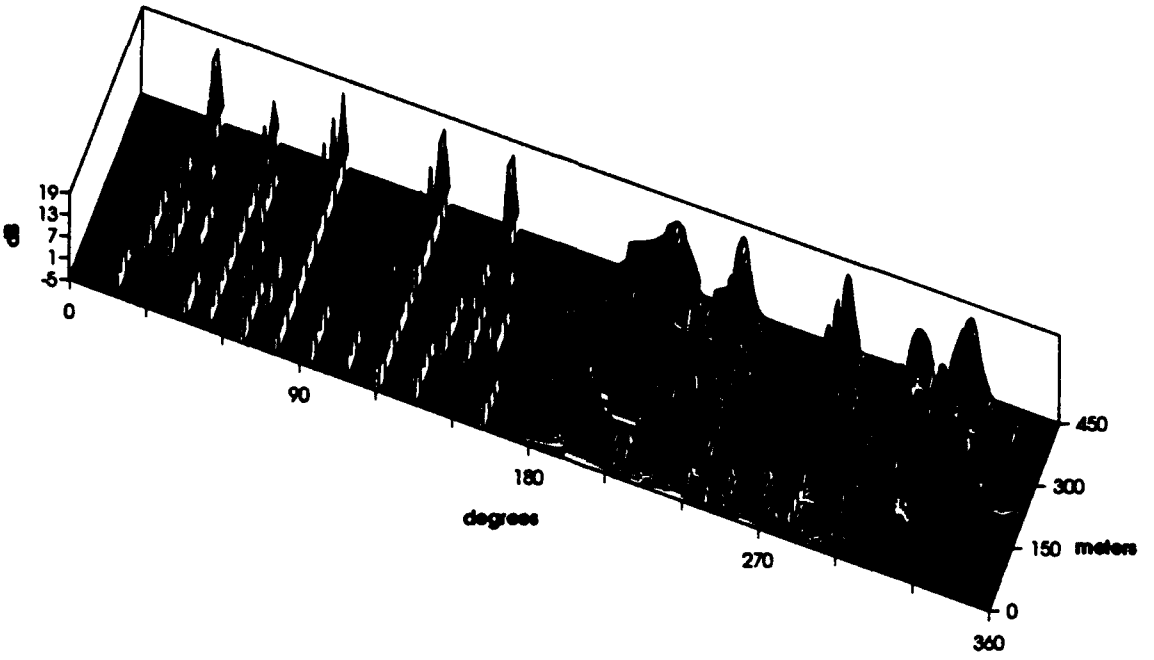

Figure 16. ALMA beamformer response to "ALMA" scatterer distribution for 2 11-element segments, 11 subarrays.

APPLICATION TO OTHER ARRAY SHAPES AND ARRAYS WITH POSITION ERRORS

The extension of ALMA beamforming to arbitrary array shapes is not envisioned because there is an implicit assumption in spatial-smoothing that the subarrays have the same relative element positions. This limitation would seem to make the technique especially unsuited to random arrays, although simulations done as part of this work have indicated that randomization of the line-array positions of a small fraction of a wavelength can be tolerated, with our without phase correction, with minimal degradation. One such example of a randomized array is that of a periodic line array with random element position errors. This case was simulated as a test of the robustness of the technique. Figure 17 shows the result, which may be compared with the error-free case shown in figure 2, for the case when uniformly distributed errors of ± 0.1 wavelength were applied to all three coordinate directions. Although there is significant degradation, the process is evidently maintaining a useful level of performance. Larger uncorrected errors were also simulated, and ± 0.1 wavelength appeared to be about the practical limit.

One can design periodic planar and volumetric array configurations for which ALMA beamforming should be applicable without violating the underlying assumptions. Such distributions can also, generally, be treated as arrays of line arrays, wherein each line could be beamformed using the ALMA algorithm.

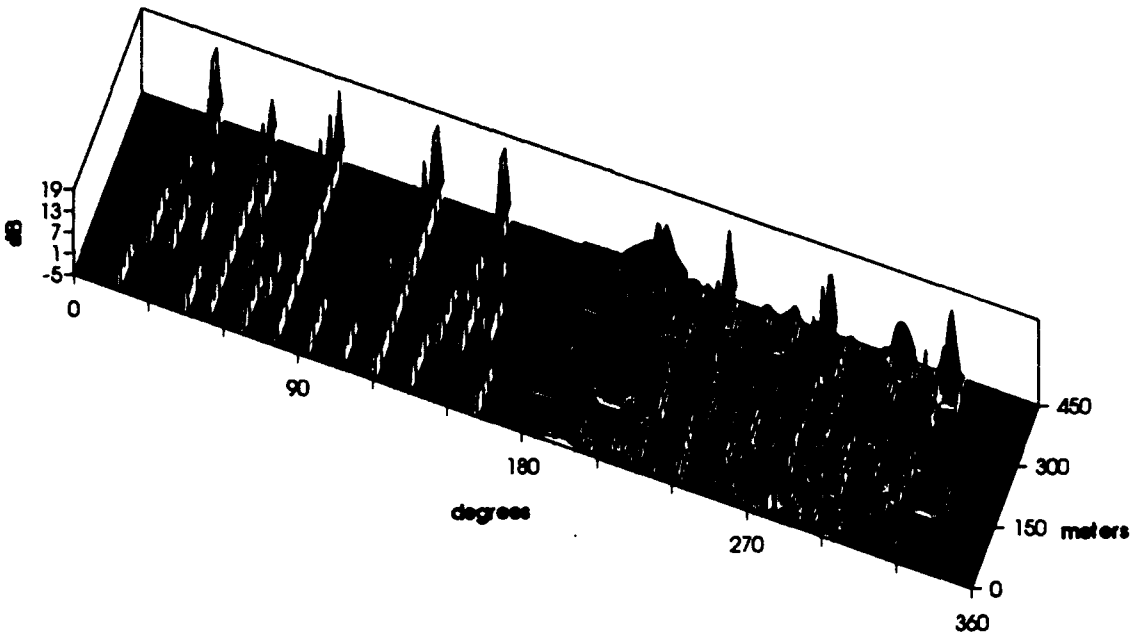

Figure 17. ALMA response with ±0.1 wavelength position errors.

Of particular interest is the question of applying ALMA to circular or cylindrical arrays. A circular array was simulated to resemble the horizontal distribution of a generic tactical array operating near 3 kHz. Ninety-six elements were spaced equally on a 3.8 m radius circle. Each element was given a directivity pattern relative to its forward axis of $(1 + \cos\theta)/2$ to attenuate signals coming from behind the array. A sector of approximately 120° was steered by rotating the distribution of active elements, making every beam essentially broadside. For each steering direction, the appropriate 31 elements were used to form 7 25-element subarrays. A beam-based adaptation was then performed using 7 beams in the covariance. For the simulation, the bandwidth of the LFM signal was taken to be 100 Hz. Figures 18 – 20 show the results of the simulation. Figure 18 shows the target distribution, and figure 19 shows the conventional response to that distribution. Note the relative lack of response in the 180- to 360-degree sector due to the element directivity. Figure 20 shows the adaptive response. In spite of the lack of perfect periodicity of the array, the adaptive result shows a definite improvement over the conventional. The fact that the aperture remains near broadside as the array is steered is highly beneficial. In an earlier attempt at simulating a circular array, a fixed aperture was steered over a 360-degree sector, and the results were quite poor except near broadside. The simulation results just presented give a preliminary indication that it should be feasible to implement the ALMA beamformer in a tactical system with beneficial results.

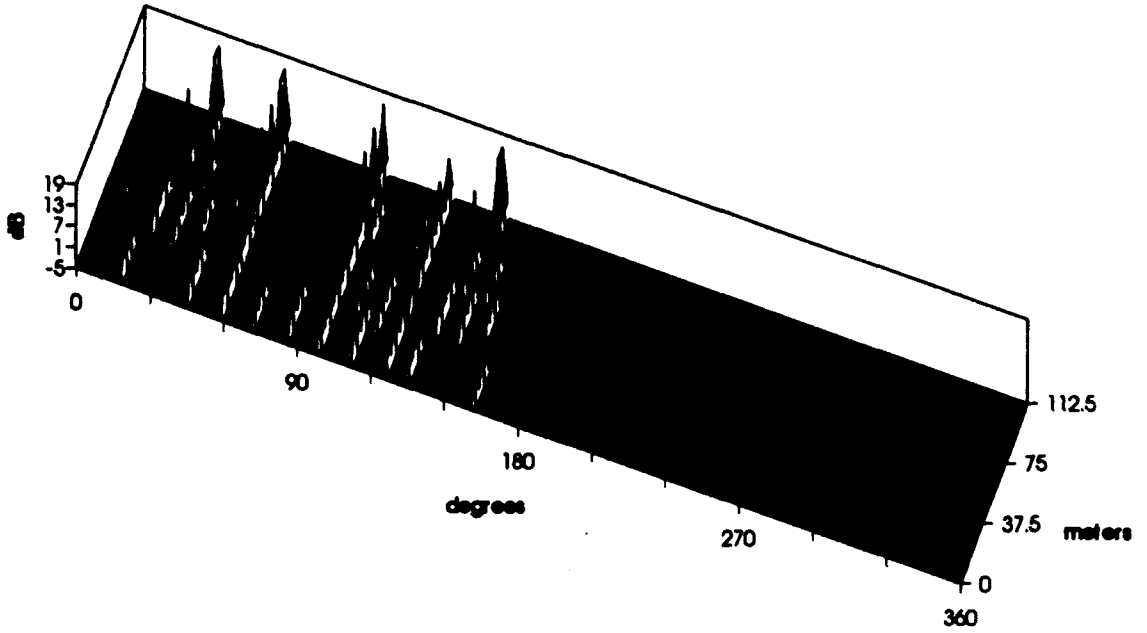

Figure 18. "ALMA" scatterer distribution for cylindrical array simulation.

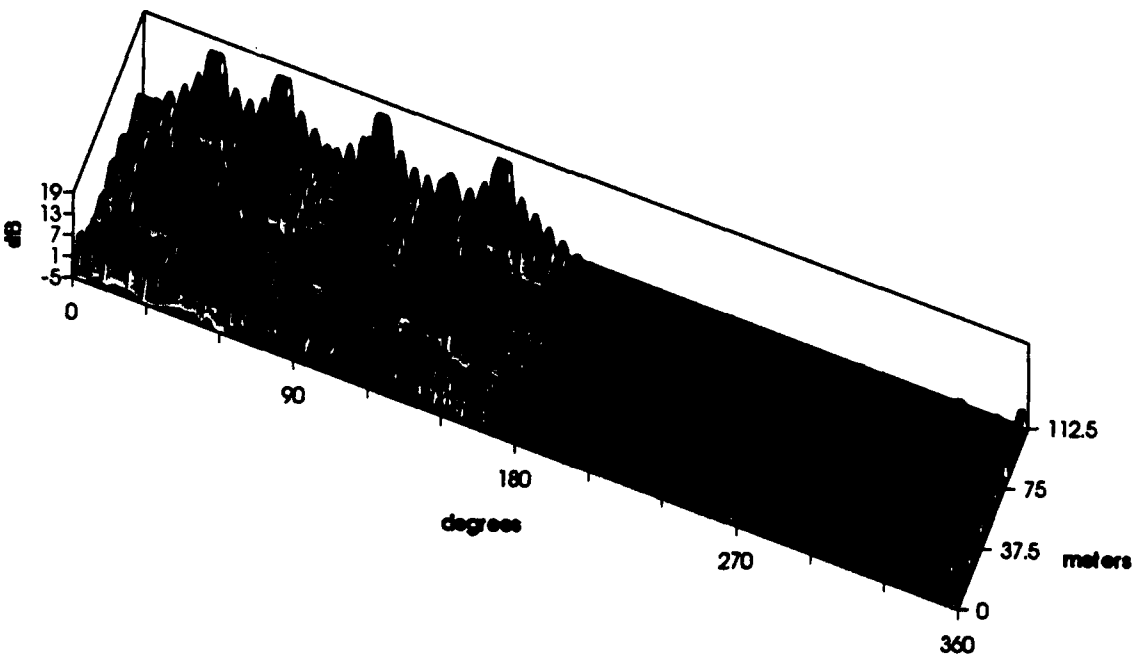

Figure 19. Cylindrical array conventional response to "ALMA" scatterer distribution.

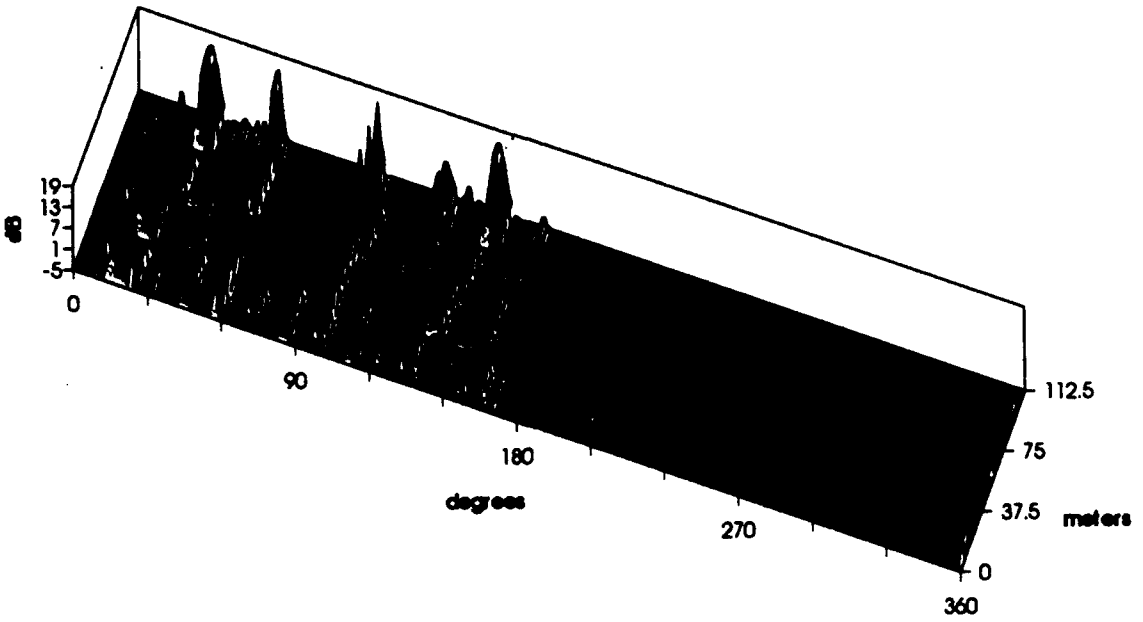

Figure 20. Cylindrical array ALMA beamformer response to "ALMA" scatterer distribution.

RELATIONSHIP OF THE MIXER OUTPUT TO REPLICA CORRELATION

We will now show that for an LFM signal the Fourier transform of the mixer output is, to a very good approximation, related to the replica correlation by a specified factor. This fact will be demonstrated using the replica as given by eq. (1) and the point target signal at the n-th element given by eq. (6).

First consider the replica correlation for a signal of length T at discrete time shifts Δ_i.

$$R(\Delta_i) = \int_0^T r(t + \Delta_i) g_n^*(t) dt \quad . \tag{74}$$

Let and $u = t + \Delta i$, $v_n = \Delta i + \tau_n$, so that $r(u)$ and $g(u)$ have the same form as eq. (1) and (6). Then the integrand is given by eq. (7) with u substituted for t, and v_n substituted for τ_n. The quadratic phase term is neglected and the original variables are restored to give the replica correlation as

$$R(\Delta_i) = e^{i\omega_0 \Delta_i} e^{i\omega_0 \tau_n} \int_0^T e^{i2a\omega_0(\Delta_i + \tau_n)t} dt \quad . \tag{75}$$

Now consider the discrete Fourier transform of the mixer output as given by eq. (7)

$$F(\omega_i) = \int_0^T r(t) g_n^*(t) e^{-i\omega_i t} dt \quad . \tag{76}$$

With the phase term linearized as above, eq. (76) can be written

$$F(\omega_i) = e^{i\omega_0\tau_n} \int_0^T e^{i(2a\omega_0\tau_n - \omega_i)t} dt \quad . \tag{77}$$

Now the discrete frequency variable is transformed to

$$\Delta_i = -\frac{\omega_i}{2a\omega_0} \quad , \tag{78}$$

and eq. (77) now becomes

$$F(\Delta_i) = e^{i\omega_0\tau_n} \int_0^T e^{i2a\omega_0(\Delta_i + \tau_n)t} dt \quad . \tag{79}$$

Thus, the replica correlation and the Fourier transform of the mixer output are related by

$$R(\Delta_i) = e^{i\omega_0\Delta_i} F(\Delta_i) \quad . \tag{80}$$

Since the factor relating the two quantities can be specified exactly for each time increment, it has been shown that the replica correlation can be obtained from the Fourier transform of the mixer output by a simple transformation.

BEAMFORMING WITH THE REPLICA CORRELATION

The time shifts required for conventional beamforming are those used in eq. (10) to obtain the frequency shifts for the ALMA algorithm. The n-th element signal must be shifted by

$$\delta\tau_n = \tau_0 - \tau_n = 2a\vec{u} \cdot (\vec{x}_n - \vec{x}_0) \quad . \tag{81}$$

The n element outputs are sampled at an interval $\Delta = \Delta_{i+1} - \Delta_i$, so that the n-th time shift equals some integral number j_n of samples plus a remainder term

$$\delta\tau_n = j_n\Delta + \varepsilon_n \quad . \tag{82}$$

For the LFM signal, the integral in eq. (75) may be solved to give an approximate result valid within the peak of the correlation function, between time samples. The result evaluated at the i-th time sample is

$$R(\Delta_i) = Te^{i\omega_0(\Delta_i + \tau_n)} \quad , \tag{83}$$

and the result at a small displacement ε from the i-th sample is

$$R(\Delta_i + \varepsilon) = Te^{i\omega_0(\Delta_i + \varepsilon + \tau_n)} = e^{i\omega_0\varepsilon} R(\Delta_i) \quad . \tag{84}$$

Thus, the correlation function at the discrete time increment can be corrected to an arbitrary offset between discrete increments by a multiplicative phase term. With this result, the beamforming procedure is analogous to the one described for the mixer-output signals. Let the vector of element responses at the i-th time sample of the correlator output be

$$V_0 = \begin{bmatrix} v_0^{(0)}(\Delta_i) \\ v_1^{(0)}(\Delta_i) \\ \vdots \\ \vdots \\ v_{N-1}^{(0)}(\Delta_i) \end{bmatrix} . \tag{85}$$

After the steering direction is chosen, the time shifts are applied to align the element time series so that the correlation peak of a point target falls in the same time-resolution cell at all the elements. The shifted element response vector is

$$V = \begin{bmatrix} v_0(\Delta_i) \\ v_1(\Delta_i) \\ \vdots \\ \vdots \\ v_{N-1}(\Delta_i) \end{bmatrix} = \begin{bmatrix} v_0^{(0)}(\Delta_i - j_0\Delta) \\ v_1^{(0)}(\Delta_i - j_1\Delta) \\ \vdots \\ \vdots \\ v_{n-1}^{(0)}(\Delta_i - j_{N-1}\Delta) \end{bmatrix} . \tag{86}$$

The shifted signals are then aligned within each resolution cell by applying a phase shift of the form seen in eq. (84). A *steering vector* is defined by

$$S = \begin{bmatrix} e^{i\omega_0\varepsilon_0} \\ e^{i\omega_0\varepsilon_1} \\ \vdots \\ \vdots \\ e^{i\omega_0\varepsilon_{N-1}} \end{bmatrix} . \tag{87}$$

Now the beamformed output is as given in eqs. (17) through (20). With conventional beamforming reduced to the same form for the replica correlation as for the mixer output, it is evident that the formulation of the adaptive algorithm will also be the same.

REPLICA-CORRELATION BEAMFORMING FOR MORE GENERAL WAVEFORMS

The equivalence that has been demonstrated for LFM between the mixer output and the replica correlation for purposes of conventional and adaptive beamforming leads to a way of formulating the ALMA beamformer for more general waveforms. Equation (84) contains a linear phase correction to transform the replica correlation at a sample point to an arbitrary point between samples. In general, the same methodology can be applied if the correction term is approximately of unit magnitude with a phase that is a known function of ε, and monotonic. Those conditions can be met for virtually any known waveform if the sampling increment is taken small enough. In the general case, then, the steering vector components would be of the form

$$s = e^{i\Phi(\varepsilon)} , \tag{88}$$

where φ must be calculated from the autocorrelation of the replica.

SUMMARY AND CONCLUSIONS

The ALMA beamforming approach has been described in detail. Results of simulations have been presented that demonstrate that the algorithms are capable of adapting to each range-resolution annulus (without time-averaging) and suppressing sidelobe interference, while preserving signals in the intended look direction. Methods of implementing spatial-smoothing for both element- and beam-based adaptive algorithms have been covered, as well as methods of applying the approach to long arrays. Finally, extensions of the approach to other array shapes and to replica-correlation-output beamforming have been discussed.

The ALMA beamforming algorithms described here have been implemented in a data-processing environment and used to process real sonar data. Those results are beyond the scope of this report. However, the author has observed in the real-data results many of the effects predicted by the simulations, including the effectiveness of the algorithm in improving the detectability of echoes through the suppression of sidelobe interference.

ALMA beamforming reduces the signal from each range-resolution cell at each array element to a single phase and amplitude (accomplished by the mixer) and applies minimum-energy adaptive methods to these quantities to adapt (without time- or range-averaging) to the scatterer distribution in each range-resolution annulus. This approach is, to the author's knowledge, a unique contribution to the field of adaptive beamforming for active signals. Based on results seen to date, ALMA beamforming offers the promise of increasing the effective array gain of modest-sized active receiving arrays to produce an effect equivalent to making the array several times longer.

REFERENCES

Cox, H., R. M. Zeskind, and M. M. Owen. 1987. "Robust Adaptive Beamforming," *IEEE Trans. Acoust., Speech, Signal Processing*, vol. ASSP-35, pp. 1365–1376 (October).

Hoerl, A. E. and R. W. Kennard. 1970. "Ridge Regression: Biased Estimation for Nonorthogonal Problems," *Technometrics*, Vol. 12 pp. 55–67 (February).

Huster, M., D. Miklovic, and S. Schmidt. 1993. "Broadband Sparse Array Image Processing for Localization and Classification in Shallow Water Environments," *Proceedings of Low Frequency Active Sonar Conference*, SACLANT Undersea Research Centre, La Spezia, Italy (24–28 May) (To be published).

Lockwood, J. C. 1986. "Adaptive Beamforming Performance with a Random Planar Array," Naval Ocean Systems Center Technical Note 1459 (July), San Diego, CA.*

Medoff, B. P., J. H. Avila, R. E. Franks, P. J. Kuekes, N. Sachs, and R. S. Schreiber. 1985. "High Speed Adaptive Signal Processing," Rome Air Development Center Technical Report No. 85–53 (March), Griffiss AFB, Rome, NY.

Shan, T-J and T. Kailath. 1985. "Adaptive Beamforming for Coherent Signals and Interference," *IEEE Trans. Acoust., Speech and Signal Proc.*, vol. ASSP-33, pp. 527–536 (June).

Vural, A. M. 1975. "An Overview of Adaptive Array Processing for Sonar Applications," *EASCON '75 Conference Proceedings*, pp. 34-A-M.

* Technical Notes (TNs) are working documents and do not represent an official policy statement of the Naval Command, Control and Ocean Surveillance Center, RDT&E Division. For further information, contact the author.

REPORT DOCUMENTATION PAGE

Form Approved
OMB No. 0704-0188

1. AGENCY USE ONLY *(Leave blank)*	2. REPORT DATE	3. REPORT TYPE AND DATES COVERED
	February 1994	Final: October 1993

4. TITLE AND SUBTITLE

ACTIVE LFM MIXER ADAPTIVE (ALMA) BEAMFORMING

5. FUNDING NUMBERS

PE: 0602314N
PROJ: RJ14B28
SUBPROJ: 73-SUB2-01
WU: DN306308

6. AUTHOR(S)

J. C. Lockwood

7. PERFORMING ORGANIZATION NAME(S) AND ADDRESS(ES)

Naval Command, Control and Ocean Surveillance Center (NCCOSC)
RDT&E Division
San Diego, CA 92152-5001

8. PERFORMING ORGANIZATION REPORT NUMBER

TR 1635

9. SPONSORING/MONITORING AGENCY NAME(S) AND ADDRESS(ES)

Office of Chief of Naval Research
Code 396600
Arlington, VA 22217

10. SPONSORING/MONITORING AGENCY REPORT NUMBER

11. SUPPLEMENTARY NOTES

This technology is covered by U. S. Patent #5,251,186 of 5 October 1993 assigned to the U. S. Government. Parties interested in licensing this technology may direct inquiries to: Harvey Fendelman, Code 0012, Legal Counsel for Patents, NCCOSC, San Diego, CA 92152-5765 (619) 553-3001

12a. DISTRIBUTION/AVAILABILITY STATEMENT

Approved for public release; distribution is unlimited.

12b. DISTRIBUTION CODE

13. ABSTRACT *(Maximum 200 words)*

This report describes the ALMA beamforming approach in detail. Results of simulations have been presented that demonstrate the algorithms can adapt to each range-resolution annulus (without time-averaging) and suppress sidelobe interference, while preserving signals in the intended look direction. Methods of implementing spatial-smoothing for both element- and beam-based adaptive algorithms have been covered, as well as methods of applying the approach to long arrays. Extensions of the approach to other array shapes and to replica-correlation-output beamforming have been discussed.

ALMA beamforming reduces the signal from each range-resolution cell at each array element to a single phase and amplitude (accomplished by the mixer) and applies minimum-energy adaptive methods to these quantities to adapt (without time- or range-averaging) to the scatterer distribution in each range-resolution annulus. This approach is a unique contribution to the field of adaptive beamforming for active signals. Based on results seen to date, ALMA beamforming offers the promise of increasing the effective array gain of modest-sized active receiving arrays to produce an effect equivalent to making the array several times larger.

14. SUBJECT TERMS	15. NUMBER OF PAGES
linear frequency modulation (LFM) active sonar adaptive beamforming	43
	16. PRICE CODE

17. SECURITY CLASSIFICATION OF REPORT	18. SECURITY CLASSIFICATION OF THIS PAGE	19. SECURITY CLASSIFICATION OF ABSTRACT	20. LIMITATION OF ABSTRACT
UNCLASSIFIED	UNCLASSIFIED	UNCLASSIFIED	SAME AS REPORT

21a. NAME OF RESPONSIBLE INDIVIDUAL	21b. TELEPHONE (Include Area Code)	21c. OFFICE SYMBOL
Dr. James C. Lockwood	(619) 553-2057	Code 734

INITIAL DISTRIBUTION

Code 0012	Patent Counsel	(1)
Code 0274B	Library	(2)
Code 0275	Archive/Stock	(6)
Code 541	N. O. Booth	(1)
Code 705	M. F. Morrison	(1)
Code 71	J. M. Holzmann	(1)
Code 7103	R. R. Smith	(1)
Code 715	P. J. Donahoe	(1)
Code 73	L. Griffith	(1)
Code 7304	W. Marsh	(1)
Code 732	R. Albrecht	(1)
Code 732	D. Grimmett	(1)
Code 732	C. Persons	(1)
Code 732	M. Rott	(1)
Code 733	T. Adams	(1)
Code 733	D. K. Barbour	(1)
Code 733	K. C. Dam	(1)
Code 733	E. P. McDaid	(1)
Code 733	R. W. Myers	(1)
Code 733	M. Reuter	(1)
Code 733	D. F. Schwartz	(1)
Code 734	S. M. Adams	(1)
Code 734	A. M. D'Amico	(1)
Code 734	A. deTorres	(1)
Code 734	J. W. Douma	(1)
Code 734	J. F. Germano	(1)
Code 734	D. T. Tran	(1)
Code 734	S. N. Tran	(1)
Code 734	W. J. Whitsell	(1)
Code 734	J. C. Lockwood	(10)
Code 78	P. M. Reeves	(1)
Code 782	R. A. Dukelow	(1)
Code 782	R. M. Hidinger	(1)

Defense Technical Information Center
Alexandria, VA 22304–6145 (4)

NCCOSC Washington Liaison Office
Washington, DC 20363–5100

Center for Naval Analyses
Alexandria, VA 22302–0268

Navy Acquisition, Research and Development
Information Center (NARDIC)
Arlington, VA 22244–5114

GIDEP Operations Center
Corona, CA 91718–8000

NCCOSC Division Detachment
Warminster, PA 18974–5000

Office of Naval Research
Arlington, VA 22217–5000

Naval Research Laboratory
Washington, DC 20375–5320 (3)

Naval Air Warfare Center
Aircraft Division
Warminster, PA 18974–0591 (5)

Naval Surface Warfare Center
Detachment White Oak
Silver Spring, MD 20903–5000 (2)

Naval Surface Warfare Center
Detachment New London
New London, CT 06320 (5)

Space and Naval Warfare Systems Command
2451 Crystal Drive
Arlington, VA 22245–5200 (2)

Advanced Research Projects Agency
Arlington, VA 22203–1714 (2)

Johns Hopkins University
Laurel, MD 20723–6099

University of Rochester
Rochester, NY 14627

University of Texas at Austin
Austin, TX 78713–8029 (5)

Alliant Technsystems, Inc.
Mukilteo, WA 98275–4844

Alliant Technsystems, Inc.
Arlington, VA 22209

Arete Associates
San Diego, CA 92064

AT&T Bell Laboratories
Arlington, VA 22202–2886

Hydroacoustics, Inc.
Rochester, NY 14692

Marine Acoustics, Inc.
Cotiut, MA 02635

Martin Marietta
Syracuse, NY 13221–4840

Orincon Corporation
San Diego, CA 92121

Raytheon Company
Portsmouth, RI 02871

Reson, Inc.
Goleta, CA 93117

Tracor Applied Sciences, Inc.
Austin, TX 78725–2050